Lighting Res. Technol. 2014; Vol. **46**: 341–353

Novel matching networks for electrodeless lamp systems

M Shao BSc, **S Huang** PhD and **W Zhao** PhD
Department of Electrical Engineering, Tsinghua University, Beijing, China

Received 19 December 2012; Revised 18 February 2013; Accepted 18 April 2013

In order to extend the length of the coaxial cable connection between an electrodeless fluorescent lamp and the associated electronic ballast, a new structure for electrodeless lamp systems is proposed in this paper. Impedance matching networks in the structure are analyzed and designed based on the transmission characteristics of coaxial cable. Efficient topologies and formulae for the matching networks are put forward. Experimental results for a 2.65 MHz electrodeless lamp system with up to 25 m of coaxial cable which validate the structure are presented.

1. Introduction

From the late 20th century, developments in semiconductor technology and changes in the standards for electromagnetic interference (EMI) have both been important in the exploitation of commercial electrodeless lamps.[1] Among the numerous issues related to electrodeless lighting systems (including the electrodeless lamp and the electronic ballast), the relative position between the lamp and the ballast has been in the ascendant. Integrating the electronic ballast into the lamp limits its rated power due to difficulties with heat rejection. This prevents the electrodeless lamp from working under high power.[2] Therefore, in actual applications of high power lighting, the lamp and the ballast are always separated and connected with a short (no more than 1 m long) coaxial cable. Nevertheless, because high power electrodeless lamps are always set at high levels, the maintenance and management of the electronic ballasts are both difficult and costly. If the length of the coaxial cable could be extended to more than 10 m, all ballasts could then be put together at a lower, safer and more manageable location, so the maintenance cost would be greatly reduced.

However, both the negative impedance of the electrodeless lamp[3,4] and the high operating frequency (more than 100 kHz) make it no easy task to match the impedance between the electronic ballast, the coaxial cable and the electrodeless lamp. OSRAM has extended the cable length of its 250 kHz electrodeless lamp ENDURA to 20 m.[5] As yet, no information has been published concerning efforts to extend the 2.65 MHz electrodeless lamp coaxial cable length. This motivated the present study on such a topic.

Section 2 describes the structure and characteristics of the electrodeless lamp and the 2.65 MHz electronic ballast and proposes a new electrodeless lighting system with an extended coaxial cable. Section 3 details the matching networks in the proposed system. Section 4 reports the experimental results. Conclusions are drawn in Section 5.

Address for correspondence: Songling Huang, Room 10314, West Main Building, Tsinghua University, Beijing 100084, China.
E-mail: huangsling@tsinghua.edu.cn

10.1177/1477153513489915

2. Proposed structure

2.1. Electrodeless lamp and ballast

The electrodeless lamp investigated in this paper is shown in Figure 1(a). The coupler is a 15-turn coil wound on a cylindrical magnetic core and is mounted inside the lamp. It is designed to transform energy from 2.65 MHz electric power supply into an electromagnetic field. The external and internal walls are seamlessly connected to form an enclosed cavity, which is filled with a buffer gas to accelerate and stabilize the formation of plasma. The main amalgam mounted in the base provides mercury atoms for the gas discharge, and the auxiliary amalgam assists the main amalgam to ignite the lamp. The phosphor powder painted on the external and internal walls absorbs ultraviolet rays and gives out visible light.

When powered on, the electrodeless lamp has two modes; the ignition mode and the operation mode. In the ignition mode, the lamp load is only the coupler coil because there is no gas discharge in the enclosed cavity. In the operation mode, a gas discharge occurs which works as a transformer shown in Figure 1(b).[6,7] The primary winding of the transformer is the coupler coil whose inductance is L_{coil} and the secondary winding is the plasma. L_{plasma} and R_{plasma} represent the inductance and resistance of the plasma, respectively. Z_{lamp} refers to the measured impedance on the primary side and is also the equivalent impedance of the lamp in the operation mode. In the ignition mode, the lamp impedance cannot be directly measured by an impedance analyzer but can be calculated from the lamp voltage and current. Thus, the experimental setup shown in

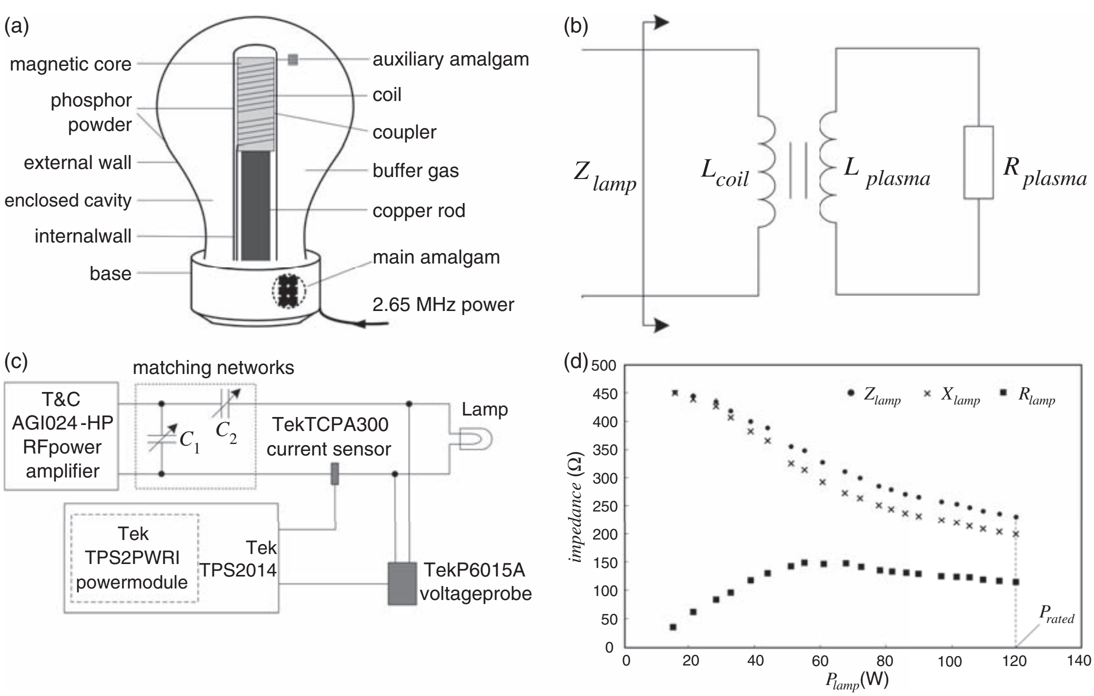

Figure 1 The electrodeless lamp, (a) structure, (b) equivalent model, (c) impedance measurement setup and (d) measured impedance characteristics under 2.65 MHz

Figure 1(c) was used to measure Z_{lamp}. The measurement results of Z_{lamp} as well as its real part R_{lamp} and imaginary part X_{lamp} versus the lamp input power P_{lamp} is shown in Figure 1(d). Z_{lamp} decreases as P_{lamp} increases, meaning that the input current will increase sharply until, finally, the ballast fails. Hence an electronic ballast is needed to stabilize the current.[8] Specifications of the electrodeless lamp under the 2.65 MHz rated condition are shown in Table 1.

The topology of the electronic ballast investigated in this paper is shown in Figure 2. To invert the direct current (DC) bus voltage V_{DC} into 2.65 MHz alternate current (AC) voltage v_s, a Class-D self-oscillating structure is adopted. The half-bridge inverter including Q_1 and Q_2 is driven by a three-winding transformer which transforms the inverter output current i_s to the driven signal of Q_1 and Q_2. When the resonant tank, the output filtering and the impedance matching stage of the electronic ballast, has an only resonant frequency of 2.65 MHz, a 2.65 MHz oscillation occurs.[9] The resonant tank is commonly designed to be the passive network of an inductor in series with a capacitor and the output terminal is in parallel with the capacitor. This causes great difficulties to the high efficiency impedance matching between the electronic ballast and a long coaxial cable.

Table 1 Specifications of the electrodeless lamp under rated condition (2.65 MHz)

Parameters	Value
Rated power	120 W
Peak ignition voltage	550 V
RMS lamp voltage	234 V
RMS lamp current	1.01 A
Z_{lamp} under rated condition	$115.7 + j200.3\,\Omega$

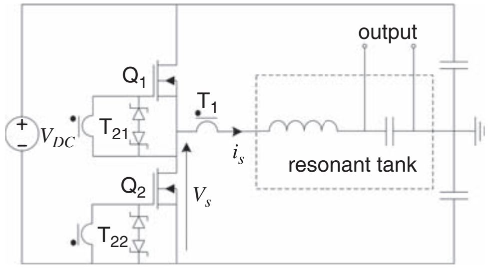

Figure 2 Topology of the 2.65 MHz self-oscillating electronic ballast

2.2. Proposed structure of the electrodeless lighting system

Given the characteristics of the electrodeless lamp, to extend the coaxial cable between the electronic ballast and the electrodeless lamp five requirements must be met. They are:

1) The input voltage of the electrodeless lamp must be high enough in the ignition mode to induce gas discharge,
2) The input power of the lamp must be the rated power of the lamp, namely, the input impedance of the electronic ballast must be the rated input impedance of the electronic ballast,
3) The input current of the electrodeless lamp should be stabilized,
4) To eliminate the reflected power caused by an impedance mismatch, the impedance matching should be implemented to transform the electrodeless lamp impedance in the operation mode to the characteristic impedance of the coaxial cable and
5) The load driven by the half bridge should be inductive to ensure the MOSFETs' zero voltage switching (ZVS).[10]

Based on these five requirements, a new electrodeless lighting system is proposed in Figure 3. The self-oscillating inverter in Figure 2 is modelled as an AC source with the electromotive force amplitude E, the internal resistance ρ and the output capacitance C_m. ρ represents the parallel value of the two MOSFETs' on resistances. C_m represents the parallel value of the two MOSFETs' output parasitic capacitances. Matching

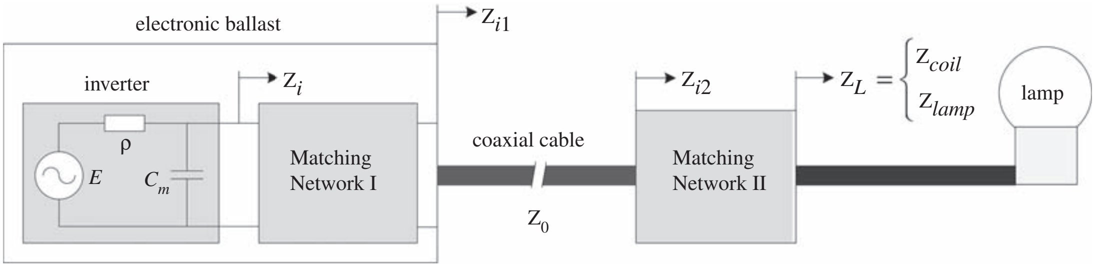

Figure 3 The proposed structure of the electrodeless lighting system

network I (MNI) connected between the inverter and the coaxial cable functions to transform the input impedance of the coaxial cable Z_{i1} into the rated load for the inverter Z_i. Also, MNI should be a 2.65 MHz band pass filter to cause self-sustained oscillation of the inverter. Therefore, the topology of MNI is specific to the electronic ballast and more complicated than the series resonant parallel load resonant tank shown in Figure 2. The second matching network, matching network II (MNII), is connected between the other terminal of the coaxial cable and the electrodeless lamp. MNII has two functions: providing a high enough input voltage to the lamp in the ignition mode and transforming the lamp impedance to the coaxial cable characteristic impedance in the operation mode. The transmission line between the MNII and the lamp is quite short and can be neglected.

2.3. Parameters of the structure

The definitions of the parameters in Figure 3 are:

Z_i: the load for the inverter, and $Z_i = R_i + jX_i$,
Z_{i1}: the load for the ballast, and $Z_{i1} = R_{i1} + jX_{i1}$,
Z_0: the characteristic impedance of the coaxial cable, $Z_0 = R_0 + jX_0$,
Z_{i2}: the load for the coaxial cable, $Z_{i2} = R_{i2} + jX_{i2}$, and
Z_L: the load for MNII, equal to the electrodeless lamp impedance. In the ignition mode, $Z_L = Z_{coil} = j\omega L_{coil}$, in the operation mode, $Z_L = Z_{lamp} = R_{lamp} + jX_{lamp}$, where $\omega = 2\pi \times 2.65 \times 10^6$ rad/s.

P_{rated} shown in Figure 1(d) is defined by the power dissipated by the lamp at the rated operation point. The rated operation point depends on the current carrying capability of the coupler, the temperature characteristics of the magnetic core and the volume of the enclosed cavity. According to the five requirements, the parameters in Figure 3 are decided as follows:

1) E, ρ and C_m. E is the amplitude of the fundamental component of v_s shown in Figure 2. v_s is a square wave with an amplitude of $0.5V_{DC}$ and an offset of $0.5V_{DC}$, so $E = 2V_{DC}/\pi$. ρ and C_m are the parallel value of the on-resistance r_{ds} and the output parasitic capacitance C_o of the two MOSFETs, respectively. ρ and C_m can be calculated using Equation (1),[10] where r_{ds} and $C_{oss|Vds} = 25\ V$ can be found in the MOSFET's datasheet.

$$\rho = \frac{1}{2} r_{ds}, \quad C_m = 2C_o = \frac{10C_{oss|Vds=25V}}{\sqrt{V_{DC}}} \tag{1}$$

2) Z_i. Among the five basic requirements, the power condition is

$$P_{rated} = \frac{E^2 R_i}{2|\rho + Z_i|^2} \cdot \eta_{MNI} \cdot \eta_{cc} \cdot \eta_{MNII} \tag{2}$$

where η_{MNI}, η_{cc}, η_{MNII} is the power transfer efficiency of the MNI, the coaxial cable and the MNII, respectively.

For given V_{DC}, Z_{i} can be determined using the ZVS optimization method of Reference 11. The basic idea is that Z_{i} should be inductive to realize half bridge ZVS. Consequently, i_{s} in Figure 2 will lag v_{s}, so when the polarity of v_{s} changes, a residual part of i_{s} still exists to discharge the output capacitance of the upcoming conducting MOSFET completely to let the MOSFET conduct under zero drain-source voltage. Meanwhile, too much residual current will increase the amplitude of i_{s} and enlarge the conduction loss, so the condition that C_{o} just be fully discharged will be adopted, as shown in Equation (3). From Equations (2) and (3), Z_{i} can be calculated.

$$\int_0^{\arctan\frac{X_i}{R_i}} \frac{E}{|\rho + Z_{\text{i}}|}\sin(\omega t)d(\omega t) = \frac{1}{2}C_{\text{m}}V_{\text{DC}} \quad (3)$$

3) $Z_{\text{i}1}$ and $Z_{\text{i}2}$. To realize full impedance matching, the lamp impedance Z_{L} should be transformed into the coaxial cable characteristic impedance by MNII, thus, the lumped impedance measured from the other terminal of the coaxial cable will also be Z_0, that is,

$$Z_{\text{i}1} = Z_{\text{i}2} = Z_0 \quad (4)$$

3. Analysis and design of matching networks

3.1. MNI

According to the location of MNI in Figure 3, the input and output characteristics are clearly shown in Figure 4. The proposed MNI is composed of subnetwork I, inductance L_{i} and reactance X_{com}. L_{i} is the inductance of Z_{i}. X_{com} is used to compensate X_0 (the reactance component of Z_0). L_{i} and X_{com} can be directly determined by the imaginary part of Z_{i} and Z_0. Thus, the function of subnetwork I is to transform R_0 (resistive of Z_0) into

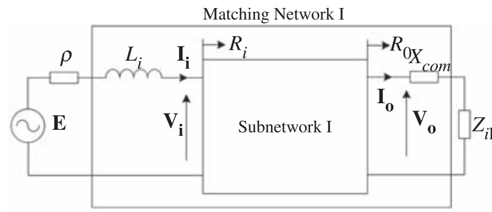

Figure 4 The structure of matching network 1

R_{i} (resistive of Z_{i}). Also, MNI should act as the frequency selective network for the self-oscillating inverter. These two main functions as well as the power transfer efficiency will be analysed here. It should be noted that C_{m} is not included in Figure 4 unlike Figure 3. The reason is that C_{m} only works in the switching transition period of the MOSFETs and just affects the ZVS control, it can be ignored when analyzing the stead-state performance of MNI.

For subnetwork I in Figure 4, $\mathbf{V_i}$ is the phasor form of the input voltage, V_i is its amplitude. So are the input current $\mathbf{I_i}$, the output voltage $\mathbf{V_o}$ and the output current $\mathbf{I_o}$. As a reactance network, subnetwork I can be built up with a basic L-section network. According to the nature of the components, two kinds of L-section network are shown in Figure 5. Figure 5(a) is the *C*-*L* low-pass type, Figure 5(b) is the *L*-*C* high-pass type.[12]

To simplify the analysis of the two L-section networks, we assume $L_{11} = L_{12}$, $C_{11} = C_{12}$. The transformation quality factor Q, the input quality factor Q_{i}, the output quality factor Q_{o} and the component quality factor Q_{L} and Q_{C} are defined as shown in Equation (5),

$$Q = \sqrt{\frac{R_{\text{i}}}{R_0} - 1}, \quad Q_i = \frac{R_i}{|X_{11}|}, \quad Q_o = \frac{|X_{12}|}{R_0}$$
$$Q_{\text{L}} = \frac{\omega L_{11}}{ESR_{L_{11}}} = \frac{\omega L_{12}}{ESR_{L_{12}}},$$
$$Q_C = \frac{1}{\omega C_{11} \times ESR_{C_{11}}} = \frac{1}{\omega C_{12} \times ESR_{C_{12}}} \quad (5)$$

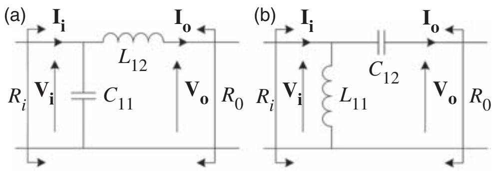

Figure 5 L-section networks (a) *C-L* low-pass type (b) *L-C* high-pass type

Where ESR_{xx} means the equivalent series resistance of component xx, and

$$\begin{aligned} X_{11} &= -(\omega C_{11})^{-1} = \omega L_{11}, \\ X_{12} &= \omega L_{12} = -(j\omega C_{12})^{-1} \end{aligned} \tag{6}$$

For impedance matching implementation and optimal efficiency, conclusions given by reference 13 as follows are helpful.

1) The formulation for the desired resistance transformation of the basic L-section network is

$$Q = Q_{\mathrm{i}} = Q_o \tag{7}$$

2) The power transfer efficiency expression of the *C-L* low-pass type and the *L-C* high-pass type are the same, shown as Equation (8). Therefore, a lower Q produces a higher efficiency. Q_{L} and Q_{C} should also be as high as possible for a higher efficiency under a given Q.

$$\eta = \left(1 - \frac{Q}{Q_C}\right)\left(1 + \frac{Q}{Q_L}\right)^{-1} \tag{8}$$

3) Under a high Q value, a multistage L-section network can be employed to reduce power loss. The maximum power transfer efficiency $\eta_{\max}$, corresponding stage quantity n_{opt} and transformation quality factor of every stage Q_n (transformation quality factor of every stage should be equal) are as shown in Equation (9), where "$\lceil\rceil$" is the rounding function. Q_{C} is neglected here because capacitors are always much less lossy than inductors.

$$\eta_{\max} \approx 1 - \frac{n_{\mathrm{opt}}\left(\Pi_{i=1}^{n_{\mathrm{opt}}} Q_i\right)^{\frac{1}{n_{\mathrm{opt}}}}}{Q_L}, \quad n_{\mathrm{opt}} = \lceil \ln Q \rceil,$$
$$Q_n = \sqrt{\left(\frac{R_i}{R_0}\right)^{\frac{1}{n_{\mathrm{opt}}}} - 1} \tag{9}$$

MNI, besides efficiently transforming the impedance, also serves to select the target operation frequency (2.65 MHz) for the self-oscillating inverter. Meanwhile, unlike the second-order resonant tank in Figure 2 starting under light load, the self-oscillating inverter in Figure 3 starts under a much heavier load, so it should be a higher-order band-pass filter for the formation of self-sustained oscillation. Therefore, at least one *C-L* low-pass type and at least one *L-C* high-pass type should be included in MNI. The stage quantity of MNI under the maximum efficiency $n_{\text{opt-1}}$ is

$$n_{\mathrm{opt}-1} = \max\left(\left\lceil \ln\sqrt{\frac{R_{\mathrm{i}}}{R_0} - 1}\right\rceil, 2\right) \tag{10}$$

The inductance and capacitance of the cascaded *C-L* low-pass type and *L-C* high-pass type L-section network is then derived by Equations (5), (6), (9) and (10), shown as Equation (11).

$$L_{11} = R_{\mathrm{i}}\left[\omega\sqrt{\left(\frac{R_{\mathrm{i}}}{R_o}\right)^{\frac{1}{n_{\mathrm{opt}-1}}} - 1}\right]^{-1}, \tag{11}$$

$$C_{12} = \left[\omega R_0\sqrt{\left(\frac{R_i}{R_o}\right)^{\frac{1}{n_{\mathrm{opt}-1}}} - 1}\right]^{-1},$$

$$L_{12} = \frac{R_0}{\omega}\sqrt{\left(\frac{R_{\mathrm{i}}}{R_o}\right)^{\frac{1}{n_{\mathrm{opt}-1}}} - 1},$$

$$C_{11} = (\omega R_{\mathrm{i}})^{-1}\sqrt{\left(\frac{R_{\mathrm{i}}}{R_o}\right)^{\frac{1}{n_{\mathrm{opt}-1}}} - 1} \tag{11}$$

In Equation (10), it can be easily found that when $n_{\text{opt}-1} > 2$, the ratio of R_i and R_0 will be more than 8.4. For the case of general RF coaxial cable and the electrodeless lamp impedance (see Figure 1(c)), the ratio of R_i and R_0 is far less than 8.4, so $n_{\text{opt}-1} = 2$, i.e. the topology of subnetwork I is only a *C-L* low-pass type cascaded with a *L-C* high-pass type, which is quite desirable.

To absorb the ZVS inductance L_i and the compensation reactance X_{com} into subnetwork I, the *L-C* high-pass type can be connected with L_i and the *C-L* low-pass type can be connected with X_{com}, the topology of MNI will then be derived as Figure 6. Also, another important consideration in this topology is that L_{12} can stabilize the output current of the inverter, like the series inductor of the resonant tank in Figure 2. The component parameters derived through Equation (11) are shown in Equation (12), where X_i has been previously determined, n_{opt} is as Equation (10), and X_{com} is equal to $-Z_0$. It should be noted that this five-component topology may be simplified to a Π type or T type network, but the efficiency advantage will be lost.

$$L_i = \frac{X_i}{\omega}, \quad L_{11} = R_i\left[\omega\sqrt{\left(\frac{R_i}{R_o}\right)^{\frac{1}{2}} - 1}\right]^{-1},$$

$$C'_{12} = \left[\omega R_0\sqrt{\left(\frac{R_i}{R_o}\right)^{\frac{1}{2}} - 1} + \omega X_0\right]^{-1}$$

$$L_{12} = \frac{R_0}{\omega}\sqrt{\left(\frac{R_i}{R_o}\right)^{\frac{1}{2}} - 1},$$

$$C_{11} = (\omega R_i)^{-1}\sqrt{\left(\frac{R_i}{R_o}\right)^{\frac{1}{2}} - 1} \tag{12}$$

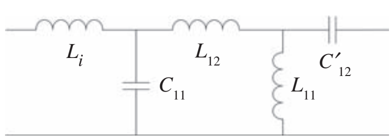

Figure 6 The topology of matching network I

3.2. MNII

For MNII, two main functions need to be considered, the impedance matching and the starting voltage of the lamp. According to matching network theory, a Π type network is proper for resistance transformation and reactance compensation. Network transmission theory will be used to discover the condition for a sufficiently high output voltage of MNII under the ignition mode.

The topology of the MNII is shown as Figure 7. It is composed of a compensation reactance $-X_{com}$ and a Π type subnetwork II. Y_{21} and Y_{23} are admittances and their corresponding reactances are Z_{21} and Z_{23}, respectively. Z_{22} is a reactance, whose admittance is Y_{22}. Y_{23} is used to compensate the reactance part of Z_L. $\mathbf{V_{i2}}$ is the phasor form of the input voltage, V_{i2} is its amplitude. So are the input current $\mathbf{I_{i2}}$, the output voltage $\mathbf{V_L}$ and the output current $\mathbf{I_L}$.

The transmission equation of the MNII is

$$\begin{bmatrix} \mathbf{V_{i2}} \\ \mathbf{I_{i2}} \end{bmatrix} = \begin{bmatrix} T_{11} & T_{12} \\ T_{21} & T_{22} \end{bmatrix} \begin{bmatrix} \mathbf{V_L} \\ \mathbf{I_L} \end{bmatrix} \tag{13}$$

Where T_{11} and T_{22} are both real, T_{12} and T_{21} are both imaginary. The elements of the transmission matrix are

$$T_{11} = 1 + Z_{22}Y_{23} \tag{14}$$

$$T_{12} = Z_{22} \tag{15}$$

$$T_{21} = Y_{21} + Y_{23} + Y_{21}Z_{22}Y_{23} \tag{16}$$

$$T_{22} = 1 + Y_{21}Z_{22} \tag{17}$$

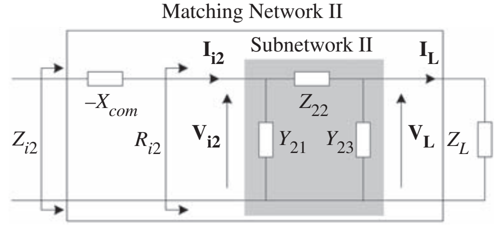

Figure 7 The topology of matching network II

As mentioned above, MNII should be resonant with L_{coil} to provide a high enough breakdown voltage for gas discharge in the ignition mode. Under resonance, the input voltage of the lamp V_{L} will be infinite. From Figure 7, V_{L} can be expressed as

$$V_{\mathrm{L}} = \frac{1}{1 + Z_{22}(Y_{\mathrm{coil}} + Y_{23})} V_{i2} \qquad (18)$$

Where $Y_{\mathrm{coil}} = 1/Z_{\mathrm{coil}}$. When resonance occurs, the denominator of Equation (18) happens to be zero. Therefore, the resonant condition can be expressed as Equation (19).

$$1 + Z_{22}(Y_{\mathrm{coil}} + Y_{23}) = 0 \qquad (19)$$

Under the operation mode, $Z_{\mathrm{L}} = Z_{\mathrm{lamp}} = R_{\mathrm{lamp}} + jX_{\mathrm{lamp}}$, R_{i2} can be deduced from Equation (13), as shown in Equation (20).

$$R_{\mathrm{i2}} = \frac{T_{11}Z_{\mathrm{lamp}} + T_{12}}{T_{21}Z_{\mathrm{lamp}} + T_{22}} \qquad (20)$$

To achieve the coaxial cable terminal impedance matching, $R_{\mathrm{i2}} = R_0$, Equations (21) and (22) can then be inferred.

$$\begin{aligned}(1 + Z_{22}Y_{23})R_{\mathrm{lamp}} &= R_0[(1 + Y_{21}Z_{22}) + j(Y_{21} + Y_{23} \\ &\quad + Y_{21}Z_{22}Y_{23})X_{\mathrm{lamp}}]\end{aligned} \qquad (21)$$

$$\begin{aligned}Z_{22} + j(1 + Z_{22}Y_{23})X_{\mathrm{lamp}} \\ = R_0(Y_{21} + Y_{23} + Y_{21}Z_{22}Y_{23})R_{\mathrm{lamp}}\end{aligned} \qquad (22)$$

By putting Equations (19), (21) and (22) together, Y_{21}, Z_{22} and Y_{23} can be solved. The reactance properties and values of MNII can then be determined.

3.3. Coaxial cable

Demands for electromagnetic shielding and EMI reduction support coaxial cable as the most cost efficient solution for electrodeless lamp system power transmission. However, the coaxial cable distributed parameters would influence the energy transfer if the impedance does not match. According to transmission line theory, the distributed parameter model of the coaxial cable is shown in Figure 8. R_0, L_0, G_0 and C_0 represent the parasitic resistance, inductance, conductance and capacitance per unit length, respectively. Z_{load} is the load connected to one terminal and Z_{in} is the lumped impedance measured from the other terminal. A one-dimension coordinate z whose origin is at the load terminal and whose positive direction goes to the load is employed, by which the coordinate of the input terminal is $-l$, where l is the coaxial cable length.

The input impedance Z_{in} can be expressed as

$$\begin{aligned}Z_{\mathrm{in}} &= Z_0 \frac{1 + \Gamma e^{-2\gamma l}}{1 - \Gamma e^{-2\gamma l}} \\ &= Z_0 \frac{Z_{\mathrm{load}} + Z_0 \tanh \gamma l}{Z_0 + Z_{\mathrm{load}} \tanh \gamma l} = R_{\mathrm{in}} + jX_{\mathrm{in}}\end{aligned} \qquad (23)$$

Where γ is the complex propagation constant, α is the attenuation constant and β is the phase constant, Γ is the reflection coefficient at the load terminal. Z_0 and γ can be calculated using Equations (24) and (25) by measuring the input impedance $Z_{\mathrm{in}} = Z_{\mathrm{ts}}$

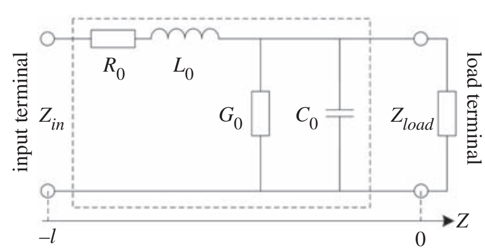

Figure 8 The distributed parameter model of coaxial cable

under $Z_{load} = 0$ and the input impedance $Z_{in} = Z_{to}$ under $Z_{load} = \infty$.

$$Z_0 = \sqrt{\frac{R_0 + j\omega L_0}{G_0 + j\omega C_0}}, \quad \Gamma = \frac{Z_L - Z_0}{Z_L + Z_0} \qquad (24)$$

$$\gamma = \sqrt{(R_0 + j\omega L_0)(G_0 + j\omega C_0)} = \alpha + j\beta \qquad (25)$$

According to the expression of Z_{in} in Equation (23), for SYV-50-1 type coaxial cable under 2.65 MHz, $Z_0 = 52.11 - j1.34$, $\alpha = 2.264 \times 10^{-3}$, the variation of R_{in} and X_{in} versus Γ for $l = 15$ m is shown in Figure 9(a). According to the definition of Γ, near $\Gamma = 0$, an increasing of Z_{load} will cause both R_{in} and X_{in} to decrease. So the coaxial cable behaves like an impedance inverter.

The transmission efficiency η_{cc} is defined by the ratio of the power dissipated by the load and what flows into the input terminal. It is related to α, l and Γ, as shown in Equation (26). η_{cc} versus l and $|\Gamma|$ is shown in Figure 9(b) for a 15 m SYV 50-1 coaxial cable, which shows that η_{cc} decreases while l or $|\Gamma|$ increases and that zero reflection coefficient ensures the highest transmission efficiency. Curves of η_{cc} versus l at fixed $|\Gamma|$ are shown in Figure 9(c). For SYV 50-1 type coaxial cable, when $|\Gamma| = 0$, the cable length should be less than 23 m to guarantee η_{cc} over 90%.

$$\eta_{cc} = \frac{1 - |\Gamma|^2}{e^{2\alpha l} - |\Gamma|^2 e^{-2\alpha l}} \qquad (26)$$

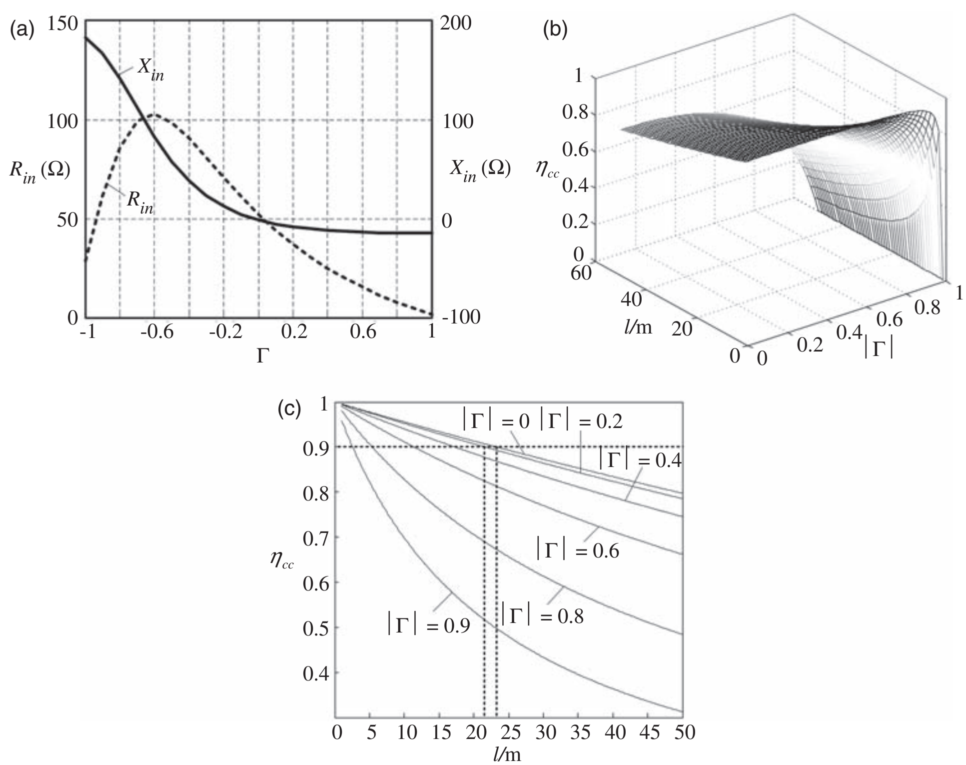

Figure 9 The coaxial cable input impedance Z_{in} and power transmission efficiency η_{cc} vs length l and load terminal reflection coefficient Γ for SYV 50-1 coaxial cable, $f = 2.65$ MHz, $\alpha = 2.264 \times 10^{-3}$, $l = 15$ m. (a) Z_{in} vs Γ, (b) η_{cc} vs l and $|\Gamma|$ and (c) η_{cc} vs l at fixed $|\Gamma|$

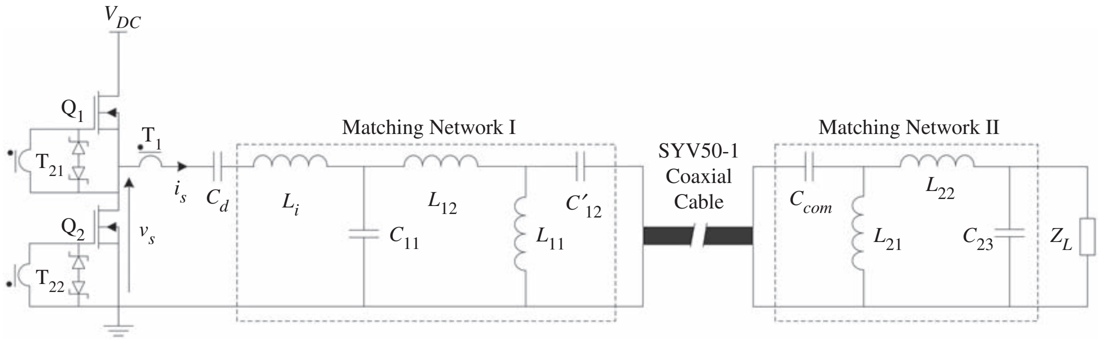

Figure 10 The experimental setup

4. Experimental verification

4.1. Experimental setup

The experimental setup is shown in Figure 10. C_d is a blocking capacitor. The parameters calculated from the analysis above are shown in Table 2. When calculating Z_i, we assume that the efficiency of MNI, MNII and the coaxial cable are all 0.95. The characteristic impedance of the coaxial cable is calculated from the Z_{ts} and Z_{to} measurement results of 15 m SYV-50-1 cable using an Agilent 4294A impedance analyzer, where under 2.65 MHz, $Z_{ts} = 28.51 + j181.9$, $Z_{to} = 1.533 - j14.68$. According to Equations (24) and (25), $Z_0 = 52.11 - j1.340$, $\gamma = (2.264 + j86.45) \times 10^{-3}$. Devices, parameters and model are listed in Table 3.

According to the coaxial cable power transfer efficiency characteristic (Figure 9(a)) and the application requirement, the experimental coaxial cable length is 5–25 m with a 5 m interval. A Tektronics TDS 2014 oscilloscope with a TPS2PWR1 power analysis module, a P6015A voltage probe and a TCPA300 current probe are used for the efficiency test.

4.2. Results and discussion

When the coaxial cable length is extended from 5 m to 25 m, the electrodeless lamp keeps igniting quickly and radiating steadily.

Table 2 Parameters under 2.65 MHz for circuit design

Parameters	Value
V_{DC}	400 V
Z_i	$204.3 + j46.89\ \Omega$
Z_{i1}	$52.11 - j1.340\ \Omega$
Z_{i2}	$52.11 - j1.340\ \Omega$
Z_0	$52.11 - j1.340\ \Omega$
γ	$(2.264 + j86.45) \times 10^{-3}$
Z_{coil}	$0.3541 + j405.3\ \Omega$
Z_{lamp} [a]	$115.7 + j200.3\ \Omega$

[a]Under rated condition.

Figure 11 shows some measurement results versus the coaxial cable length l, including: The input power of the inverter and that of the lamp (Figure 11(a)), the amplitude and phase angle of the reflection coefficient Γ at the junction of coaxial cable and MNII (Figure 11(b)), the efficiency of MNI, coaxial cable and MNII (Figure 11(c)), and the efficiency of the inverter and the whole system (Figure 11(d)).

Figure 11(a) shows that, with the coaxial cable length increasing, the input power of the inverter increases and that of the lamp decreases slightly. This indicates an internal mechanism conducive to the stability of lamp power existing in the proposed ballast structure. When the input power of the lamp decreases with the coaxial cable length increasing, the lamp impedance increases, R_{i2} decreases due to the negative impedance inverting characteristic of MNII,

Table 3 Devices, parameters and model

Device	Parameters	Model	
Q_1, Q_2	$r_{ds\|id=0.8A} = 2\,\Omega$ $C_{oss\|Vds=25V} = 55$ pF	Fairchild FQPF5N60C	
T_1	1.663 μH	Core I[a]	5Ts
T_{21},T_{22}	3.326 μH		10Ts
L_i	5.221 μH, $Q = 97.54$	Core II[a], 13Ts	
L_{11}	Please provide the volume number for Ref. 6.	Core III[a], 18Ts	
L_{12}	3.098 μH, $Q = 113.6$	Core II, 10Ts	
L_{21}	15.06 μH, $Q = 68.93$	Core III, 20Ts	
L_{22}	7.773 μH, $Q = 92.15$	Core II, 16Ts	
C_d	1.505 nF, $Q > 200$	TDK[b] CK45-RR $\pm$ 10% 1–3 kV ceramic capacitors	
C_{11}	291.1 pF, $Q > 200$		
C_{12}	1.195 nF, $Q > 200$		
C_{com}	4.482 nF, $Q > 200$		
C_{23}	594.7 pF, $Q > 200$		

[a]Core I, II and III are all Ni-Zn ferrite cores with relative magnetic permeability of around 60. Their sizes (outer diameter $\times$ inner diameter $\times$ thickness) (mm) are $24.3 \times 13.9 \times 23.7$, $23.4 \times 13.9 \times 15.9$, $13.4 \times 6.89 \times 5.44$, respectively. Ts means turns.
b1.5 nF for C_d, 270 pF + 2 $\times$ 10 pF for C_{11}, 1.2 nF for C_{12}, 3.3 nF + 1.2 nF for C_{com} and 330 pF + 270 pF for C_{23}.

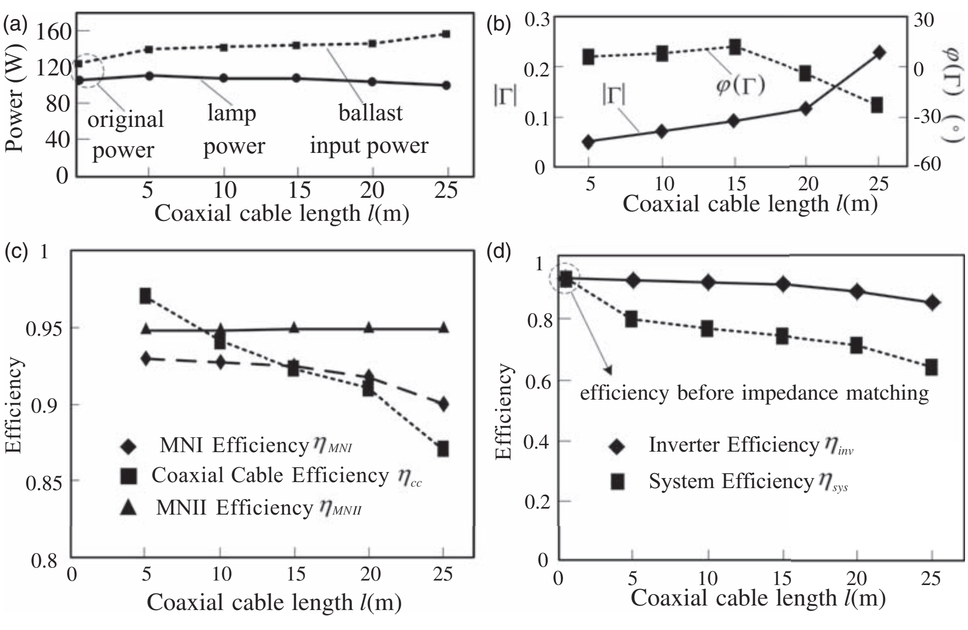

Figure 11 Experimental results (a) inverter input power and lamp input power vs l, (b) reflection coefficient vs l, (c) efficiency of MNI, MNII and coaxial cable vs l and (d) efficiency of inverter and whole system vs l

and then Γ decreases ($\Gamma < 0$). According to Figure 9(a), R_{i1} increases. Finally, R_i decreases because MNI is also an impedance inverter, what follows is an increase of the inverter input power. It can be predicted that, when the lamp input power increases, the inverter input power will decrease to reduce the lamp power. In practical applications, such a lamp power stabilizing mechanism is necessary for the extension of the coaxial cable.

Figure 11(b) shows that, with the coaxial cable length increasing, the amplitude of the reflection coefficient gradually increases, while the angle of the reflection coefficient varies from zero, which indicates the gradual deterioration of the matching degree. This is because with the coaxial cable length increasing, the input power of the lamp is reduced and the lamp impedance is changed. It can be concluded that the maximum coaxial cable length is mainly decided by the power loss on the coaxial cable. Therefore, to operate at longer distances with the same loss, a larger diameter coaxial cable can be used because the loss per meter would be lower for a larger diameter cable.

Figure 11(c) shows that, with the increasing coaxial cable length, η_{MNI} and η_{cc} decrease while η_{MNII} remains almost unchanged. The increased power loss on MNI is caused by the increased input power of the MNI and the variation of Z_{i1}. Due to the worsening terminal impedance mismatch, η_{cc} decreases sharply between 20 m and 25 m. Meanwhile, η_{cc} declines fast and becomes the lowest of the three efficiencies at $l = 15$ m.

Figure 11(d) shows that the inverter efficiency and the whole system efficiency decrease gradually as the coaxial cable length increases. The reason for the reduction of inverter efficiency is the increased input power of the inverter, and more important, the gradual disappearance of ZVS caused by the change of Z_{i}. Due to ZVS, the inverter efficiency decreases slowly from 93.5% to 89.5% as coaxial cable length extends from 5 m to 20 m. When the length reaches 25 m, the inverter efficiency rapidly decreases to 85.6%, which indicates the vanishing of ZVS. The role that ZVS plays in such a wide range of 5–20 m is quite necessary and nearly enough for basic application.

Under $l = 5$ m, the overall efficiency of the system η_{sys} is 79.6%, when the length increases to 20 m, η_{sys} decreases to 71.0%, which seems unsatisfactory. However, for general applications, this efficiency is still reasonable and advantageous. Firstly, even with around 30% power loses, the luminous efficiency is still around 60 lm/W. Secondly and more importantly, besides the great convenience brought by the extended coaxial cable length, the maintenance cost reduction can sufficiently cover the power loss expenses. Finally, for $l \leq 20$ m, the temperature rise caused by the loss is not obvious and the overall system has good reliability. For street and building lighting applications, a 20 m length is more than enough.

5. Conclusions

In this paper, a new structure for an electrodeless lamp system is proposed in order to extend the coaxial cable connected between the electronic ballast and the electrodeless lamp. Two new matching networks, MNI and MNII, are introduced in this structure. By analyzing the targets of both matching networks and investigating the basic L-section matching networks, a multistage L-section network for MNI and a Π network for MNII as well as formulas for their component values (Equations (12), (19), (21) and (22)) are put forward. Experimental results show that a 2.65 MHz electrodeless lighting system with up to 20 m of coaxial cable can work well and both efficiencies are around 90%. The overall efficiency of the ballast system decreases from 79.6% to 71.0% as the coaxial cable length extends from 5 m to 20 m, which seems unsatisfactory, but the whole electrodeless lamp system still possesses relatively advantageous luminous efficiency, the ballast maintains the usual reliability, brings great convenience and reduces the maintenance cost. One can expect to achieve higher efficiency using higher quality inductors and a larger diameter coaxial cable. Also, the proposed structure has some value for other kinds of gas discharge light sources, such as general fluorescent lamps, high intensity discharge lamps, metal halide lamps, etc.

Funding

This work was supported by the Chinese MRW S and T Research and Development Program (J2011Z001) and the Shenhua Group and Tsinghua University Strategic Cooperation Basic Research Program (20112000507).

References

1 Wharmby DO. Electrodeless lamps for lighting: A review. *IEE Proceedings A: Science, Measurement and Technology* 1993; 11: 465–473.
2 Nerone LR. Analysis and design of a self-oscillating class E ballast for compact fluorescent lamps. *IEEE Transactions Industrial Electronics* 2001; 2: 151–160.
3 Chen YM, Chen DH. *Simulation the impedance of electrodeless fluorescent lamp*: *Proceedings of the IEEE Industrial Applications Society*. Tampa, USA, 2006.
4 Nerone LR, Qureshi AH. *Mathematical modeling and optimization of electrodeless low-pressure, discharge system*: *Proceedings of the IEEE Power Electronics Specialists Conference*, University of Washington, Seattle, WA, 1993.
5 OSRAM Gmbh, Retrieved 2 April 2013, from http://www.osram.com/osram_com/products/lamps/compact-fluorescent-lamps/osram-endura/index.jsp.
6 Lister GG, Cox M. Modeling of inductively coupled discharges with internal and external coils. *Plasma Sources Science and Technology* 1992; 1: 67–73.
7 Chagas NB, Silva MFD, Schlittler ME, Fraytag J, do Prado RN, Bisogno FE. *Electrodeless fluorescent lamps model operated at high frequency*: *Proceedings of the IEEE Industrial Electronics Society*, Gdansk, Poland, 2011.
8 Kazimierczuk MK, Szaraniec W. Electronic ballast for fluorescent lamps. *IEEE Transactions on Power Electronics* 1993; 4: 386–395.
9 Lin RL, Wang ZQ. 2.65 MHz self-oscillating electronic ballast with constant-lamp-current control for metal halide lamp. *IEEE Transactions on Power Electronics* 2007; 3: 839–844.
10 Nerone LR. Design of a 2.5-MHz, soft-switching, class-D converter for electrodeless lighting. *IEEE Transactions on Power Electronics* 1997; 3: 507–516.
11 Shao MS, Huang SL, Zhao W, Wang CQ, Dong JR, Wang ZJ. Parameter optimization for 2.65 MHz electrodeless ballast. *Journal of Tsinghua University* 2011; 7: 928–932.
12 Thompson M, Fidler JK. Determination of the impedance matching domain of impedance matching networks. *IEEE Transactions on Circuits and Systems I: Regular Papers* 2004; 10: 2098–2106.
13 Han YH, Perreault DJ. Analysis and design of high efficiency matching networks. *IEEE Transactions on Power Electronics* 2006; 5: 1484–1491.